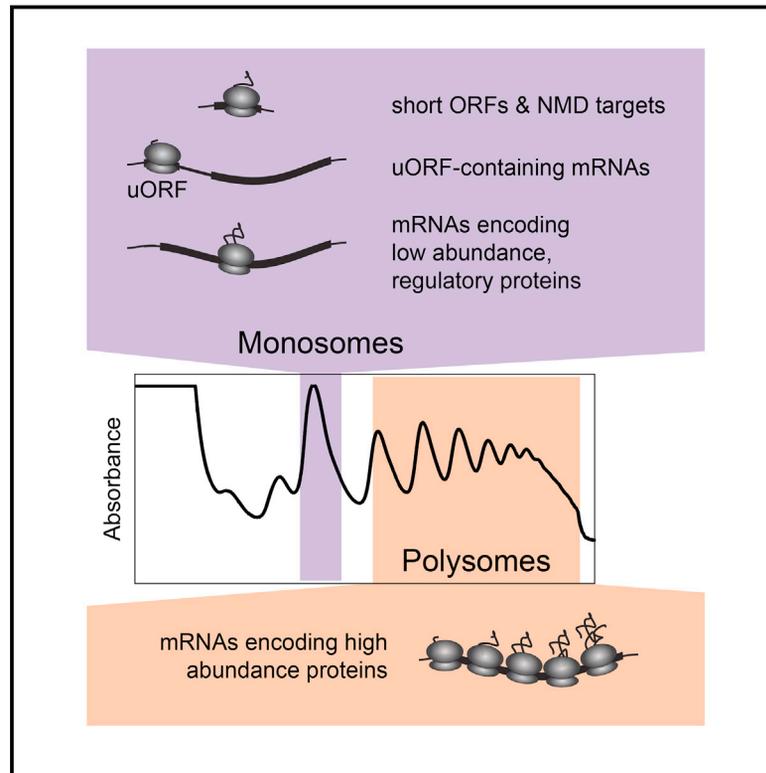# Cell

Redefining the Translational Status of 80S Monosomes

Graphical Abstract

Authors

Erin E. Heyer, Melissa J. Moore

Correspondence

melissa.moore@umassmed.edu

In Brief

Ribosome profiling in *Saccharomyces cerevisiae* reveals that the vast majority of 80S monosomes actively contribute to the translation of nonsense-mediated decay targets, open reading frames for which elongation time is substantially shorter than initiation time, and mRNAs encoding low-abundance regulatory proteins.

Highlights

- Most monosomes are actively elongating

- Monosomes translate short ORFs, uORFs, and NMD targets

- Initiation versus elongation time determines monosome versus polysome occupancy

- Low-abundance regulatory proteins are synthesized by monosomes

Accession Numbers

GSE76117

CrossMark

CellPress

Article

Redefining the Translational Status of 80S Monosomes

Erin E. Heyer[1] and Melissa J. Moore[1,*]

[1]Howard Hughes Medical Institute, RNA Therapeutics Institute and Department of Biochemistry and Molecular Pharmacology, University of Massachusetts Medical School, Worcester, MA 01605, USA
*Correspondence: melissa.moore@umassmed.edu
http://dx.doi.org/10.1016/j.cell.2016.01.003

SUMMARY

Fully assembled ribosomes exist in two populations: polysomes and monosomes. While the former has been studied extensively, to what extent translation occurs on monosomes and its importance for overall translational output remain controversial. Here, we used ribosome profiling to examine the translational status of 80S monosomes in *Saccharomyces cerevisiae*. We found that the vast majority of 80S monosomes are elongating, not initiating. Further, most mRNAs exhibit some degree of monosome occupancy, with monosomes predominating on nonsense-mediated decay (NMD) targets, upstream open reading frames (uORFs), canonical ORFs shorter than ∼590 nt, and ORFs for which the total time required to complete elongation is substantially shorter than that required for initiation. Importantly, mRNAs encoding low-abundance regulatory proteins tend to be enriched in the monosome fraction. Our data highlight the importance of monosomes for the translation of highly regulated mRNAs.

INTRODUCTION

The cytoplasm contains two populations of ribosomes: polysomes and monosomes. Polysomes consist of mRNAs occupied by two or more ribosomes, whereas monosomes are a mix of mRNAs bound by a single ribosome plus "vacant couples" wherein the large and small ribosomal subunits stably associate in the absence of mRNA (Noll et al., 1973). Ample evidence from radioactive amino acid incorporation studies indicates that the vast majority of new peptide bonds are formed on polysomes (Warner and Knopf, 2002; Noll, 2008). Thus, polysomes are generally equated with the translationally active mRNA pool, with monosomes often presumed to be newly assembled at the start codon and therefore translationally inactive (for examples, see Van Der Kelen et al., 2009; Aspden et al., 2014). Nonetheless, some fraction of monosomes must be translationally active. For example, the first or "pioneer" round of translation on any newly transcribed mRNA necessarily involves translation by a single ribosome until it has moved far enough to allow a second ribosome to assemble at the start codon. Further, the average distance between elongating ribosomes in *Saccharomyces*

cerevisiae has been estimated to be >100 nt (Arava et al., 2003; Shah et al., 2013). With such spacing, some open reading frames (ORFs) (e.g., RPL41A and RPL41B, each 78 nt) are so short that they should be occupied by just one ribosome (Yu and Warner, 2001). Consistent with this, *S. cerevisiae* mRNAs with very short ORFs cosediment predominantly with 80S monosomes (Arava et al., 2003). Notably, that study also revealed that several longer ORF mRNAs known to be translationally regulated (e.g., GCN4, CPA1, and ICY2) are primarily monosome associated.

Ribosome profiling enables the precise mapping of ribosome positions on mRNAs undergoing active translation (Ingolia et al., 2009). Here, we adapted this protocol to specifically examine the translational status of 80S monosomes in *S. cerevisiae*. We provide definitive evidence that the vast majority of monosomes are in the act of elongation, not initiation. As expected, monosomes predominate on nonsense-mediated decay (NMD) targets, including unspliced transcripts. Transcriptome-wide, relative polysome and monosome occupancy is a function of initiation versus total elongation time. That is, if initiation is faster than elongation, an mRNA will be predominantly polysome associated. Conversely, if initiation is much slower than elongation, an mRNA will be predominantly monosome associated. A high initiation:elongation ratio can be driven either by ORF length or by slow initiation rate, often indicative of translation regulation. Thus, in addition to synthesizing extremely short proteins, monosomes also translate key regulatory proteins, such as transcription factors, kinases, and phosphatases. Such regulatory factors are often transiently expressed (i.e., have short mRNA and protein half-lives) at very low levels. Therefore, relative monosome:polysome association may prove a useful metric for identifying and studying mRNAs subject to negative translation regulation.

RESULTS

Monosome, Polysome, and Global Footprinting

To generate monosome- and polysome-specific footprints, we took multiple precautions to ensure that the ribosome footprints we isolated accurately reflect intracellular conditions (Figure 1). To minimize ribosome movement during sample workup, we briefly incubated log phase cultures with 100 μg/ml cycloheximide prior to rapid collection by vacuum filtration and immediate resuspension in ice-cold lysis buffer and performed all subsequent steps at 4°C (Ingolia et al., 2009). To preserve polysome integrity, we lysed cells by vortexing with glass beads rather
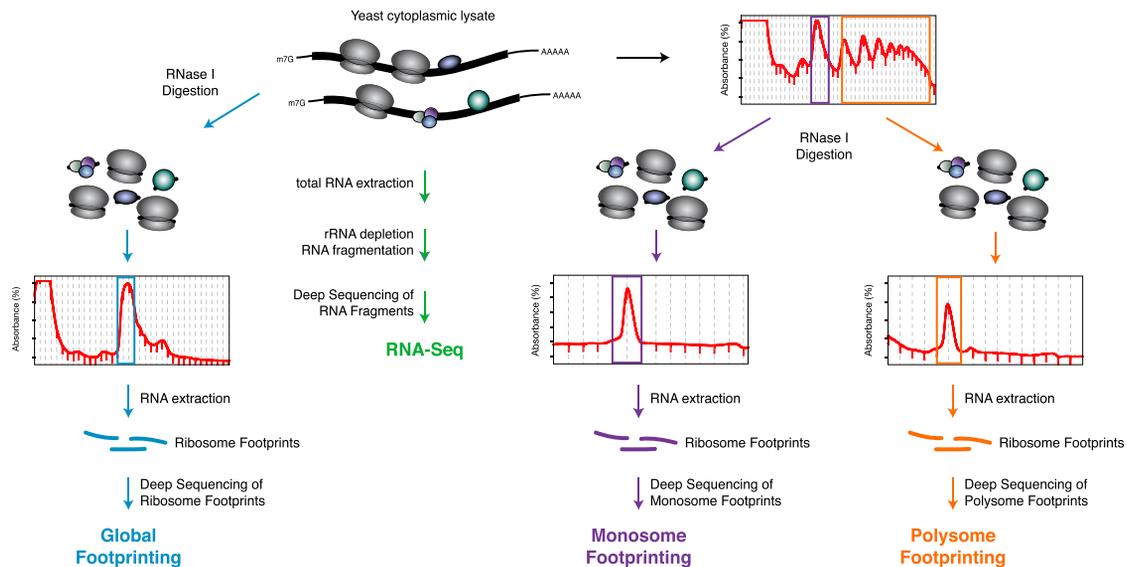
Figure 1. Experimental Scheme
See also Table S1.

than ball milling, as ball milling tends to shear polysomes and thereby artificially increase the monosome fraction. We also excluded detergent (e.g., Triton X-100) as it led to excessive foaming and poor cell lysis. Because efficient extraction of membrane-bound polysomes requires detergent (Potter and Nicchitta, 2002), we expected cytoplasmic species to predominate in our lysates. Although Mg^{2+} concentrations up to 30 mM are often used when preparing yeast extract for polysome profiling (Bhattacharya et al., 2010), $[Mg^{2+}]$ in excess of 8 mM can drive vacant couple formation (Favaudon and Pochon, 1976); therefore, we limited total $[Mg^{2+}]$ to 5 mM in all experiments.

For global ribosome profiling (Figure 1, left), cell lysates are digested with RNase I prior to ribosome isolation (Ingolia et al., 2009). Consequently, the entire ribosome population is sampled without regard to monosome or polysome status. To instead generate monosome- and polysome-specific footprints, we first separated the two populations on a 6%–38% (w/v) sucrose gradient. These gradients were centrifuged for a time sufficient to sediment the 80S monosome peak to the middle fractions, allowing both monosomes and polysomes to be collected with optimal separation between the two pools. These conditions also allowed for clean separation between monosomes and 48S initiation complexes that, although unlikely, could leave mRNA footprints upon RNase I digestion (Aspden et al., 2014; Ingolia et al., 2014). Pooled fractions were then separately digested with RNase I prior to loading on a second sucrose gradient (Figure 1, middle and right), ensuring that any mRNA fragments obtained were bona fide ribosome footprints and not similarly sized protected fragments originating from non-ribosome-bound positions on the intact monosome or polysome-bound mRNAs isolated from the first gradient. We also generated RNA sequencing (RNA-seq) libraries from total lysate RNA extracted prior to gradient fractionation.

For both biological replicates of isolated monosomes and polysomes, ∼80%–90% of uniquely mapping reads post-

ncRNA removal aligned to the sacCer3 genome (Table S1), with 5,045 of 6,692 annotated ORFs having at least ten reads in all four libraries. Scatterplots comparing either total ribosome occupancy per ORF (reads per million mapped; RPM) or ribosome density per ORF (reads per kilobase per million mapped; RPKM) revealed high correlations between biological replicates (Pearson coefficient > 0.99) (Figure S1). Thus, our monosome- and polysome-specific ribosome profiling data were highly reproducible and covered the vast majority (75%) of annotated ORFs.

Ribosome Position Analysis
When aggregated across all coding sequence (CDS) genes, ribosome footprints tend to be highly enriched at ORF 5′ ends and then sharply decrease before reaching a plateau that persists throughout the remainder of the ORF (Ingolia et al., 2009). Both metagene and aggregation plots of our global ribosome footprints replicated these features (Figures 2A and 2B, left). Monosome and polysome plots, however, were distinctly different (Figures 2A and 2B, middle and right). Whereas both exhibited ORF 5′ end enrichment, this enrichment was much more pronounced for monosomes and much less pronounced for polysomes than the global pattern. Further, the plateau was lower for monosomes and higher for polysomes than the global plateau. Therefore, monosomes and polysomes make distinct contributions to the global ribosome footprint pattern.

High monosome occupancy at ORF 5′ ends might suggest that a large fraction is in the process of initiation with tRNA^{met} in the P site. Because our double sedimentation strategy strongly disfavored free tRNA contamination in our footprinting libraries, any tRNA fragments in our libraries likely originated from stably bound tRNAs. In both monosome and polysome libraries, very similar fractions of tRNA-mapping reads (0.76%–1.03% Mono; 0.62%–1.08% Poly) corresponded to tRNA^{met} (Table S2), indicating there was no major difference in tRNA^{met} association

between monosomes and polysomes. Further, only 7% of monosome 28-nt reads were positioned over canonical ORF start codons, compared to 2% for polysomes. All other 28-nt reads mapping to canonical ORFs (93% and 98%, respectively) mapped to internal codon positions, demonstrating that most monosomes are in the process of elongation.

Further evidence for elongating monosomes came from aggregating 28-nt read 5′ end positions relative to the start codon. Both monosome and polysome footprints exhibited the 3-nt phasing characteristic of elongating ribosomes (Figure 2B, inset), and for both populations, this strong phasing continued all the way to the stop codon (Figure 2C, inset). Among all 6,692 annotated CDS genes, 5,029 (75%) had more than five 28-nt monosome footprints in each biological replicate indicative of elongation (i.e., P site inside the ORF). Thus, most monosomes (93%) were in the process of elongation, with most genes (75%) having multiple 28-nt monosome footprints within the ORF. We conclude that the preponderance of 80S monosomes in our samples were translationally active and that at least a fraction of elongation events on most mRNAs occurs while the mRNA is occupied by a single ribosome.

A prominent difference between the monosome and polysome aggregation plots occurs across codons 9–36 (Figure 2B). Whereas monosome read coverage decreased ∼3-fold over this region (5′ ends at nucleotide positions +12 to +93), polysome read coverage remained relatively even. These same patterns were observed when aggregation plots were limited to cytoplasmic mRNAs (see below; Figures S2C–S2F). Likely explanations for these different patterns are discussed below. Another difference between the aggregation plots occurred at ORF 3′ ends, where monosome reads exhibited a slight uptick (∼1.5-fold) over the last 100 nt, while polysome reads did not (Figure 2C). This uptick in monosome reads was even more pronounced in aggregation plots limited to mRNAs that were otherwise polysome enriched (Figures S2G and S2H). This signal could originate from the final ribosome on an otherwise polysome-associated mRNA as that ribosome completes translation prior to or coincident with mRNA degradation (Pelechano et al., 2015).

Features common to both monosome and polysome aggregation plots were (1) strong peaks at codons 1 and 5 (Figure 2B, labeled in right inset) and (2) a 4- rather than 3-nt gap between the last coding position peak and final peak over the stop codon (Figure 2C, inset). Because the +5 codon peak did not disappear when aggregation plots were normalized so that each gene contributed equally (Figures S2A and S2D), it was a general feature of our libraries and not due to any single gene or small gene subset. Thus, +5 pausing may be a general post-initiation feature in both yeast and mammals, where it was recently attributed to exit tunnel geometry (Han et al., 2014). The offset peak at ORF 3′ ends was also apparent in normalized aggregation plots (Figures S2B and S2F), indicating its generality. This previously observed spacing (Guydosh and Green, 2014) may be due to mRNA compaction during termination (Brown et al., 2015). Thus, with regard to these previously characterized features at the 5′ and 3′ ends of ORFs, we could detect no differences between the monosome and polysome populations.

To determine if the transcriptome-wide patterns accurately represented footprint patterns across single genes, we next examined individual ORFs. As expected from the metagene and aggregation plots, monosome footprints on many ORFs predominated at and immediately downstream of the start codon, with polysome footprints exhibiting much higher coverage across the entire ORF (e.g., SHM2 and RHR2; Figures 2D and 2E). Other genes, however, exhibited very similar patterns between the monosome, polysome, and global libraries. Some such genes encoded long and abundant proteins (e.g., actin/ACT1 and RPL16B; Figures 2F and 2G). Hence, some mRNA molecules encoding even highly abundant housekeeping genes are apparently translated by monosomes.

Features of Monosome- and Polysome-Enriched mRNAs
Next, we used the differential expression package DESeq2 (Love et al., 2014) to compute monosome versus polysome fold enrichment for each mRNA (monosome:polysome score). For cytoplasmic mRNAs, our data paralleled the previous microarray estimate of ribosome number per mRNA (Arava et al., 2003), with monosome:polysome scores increasing as estimated ribosome number decreased (Figure S3A). This relationship did not exist, however, for membrane-associated mRNAs, which were highly skewed toward monosome occupancy (Figure S3B). For these mRNAs, monosome footprints accumulated over and immediately downstream of predicted signal sequences (Figures S3C and S3D). This fits the long-standing model of ER protein import (Figure S3E), where the signal sequence is first translated by a single cytoplasmic ribosome prior to signal recognition particle (SRP) recruitment and membrane engagement. Because membrane-associated polysomes were likely undersampled due to lack of detergent in our cell lysis procedure, we limited all subsequent analyses to the 4,342 mRNAs for which no evidence exists of membrane association (i.e., cytoplasmic mRNAs).

A major determinant of ribosome number per mRNA is ORF length (Arava et al., 2003). Consistent with this, a scatterplot of monosome:polysome score versus ORF length revealed a strong inverse relationship, with shorter ORFs being more monosome-associated than longer ORFs (Figure 3A). Mean and median monosome:polysome scores of ordered bins each containing 50 genes revealed this relationship to be particularly strong and nearly linear for ORFs ≤590 nts (Figures 3B and S3F). Thus, the shortest canonical ORFs in CDS genes tend to be occupied by a single ribosome.

Besides short canonical ORFs, two other classes of short ORFs are sORFs (short <300 nt ORFs in transcripts not originally annotated as protein-coding genes [Smith et al., 2014]) and uORFs (ORFs upstream of canonical ORFs [Ingolia et al., 2009]). Both classes were strongly biased toward monosome occupancy (Figure 3C). Like short canonical ORFs, sORFs exhibited a negative correlation between ORF length and monosome:polysome read ratio; accordingly, sORFs are likely bona fide protein-coding genes translated predominantly by monosomes. Strikingly, a different behavior was observed for uORFs. Consistent with all currently annotated uORFs in non-membrane genes being <250 nt, the population as a whole was strongly biased toward monosome occupancy (Figure 3C). However, no relationship was detectable between monosome enrichment and
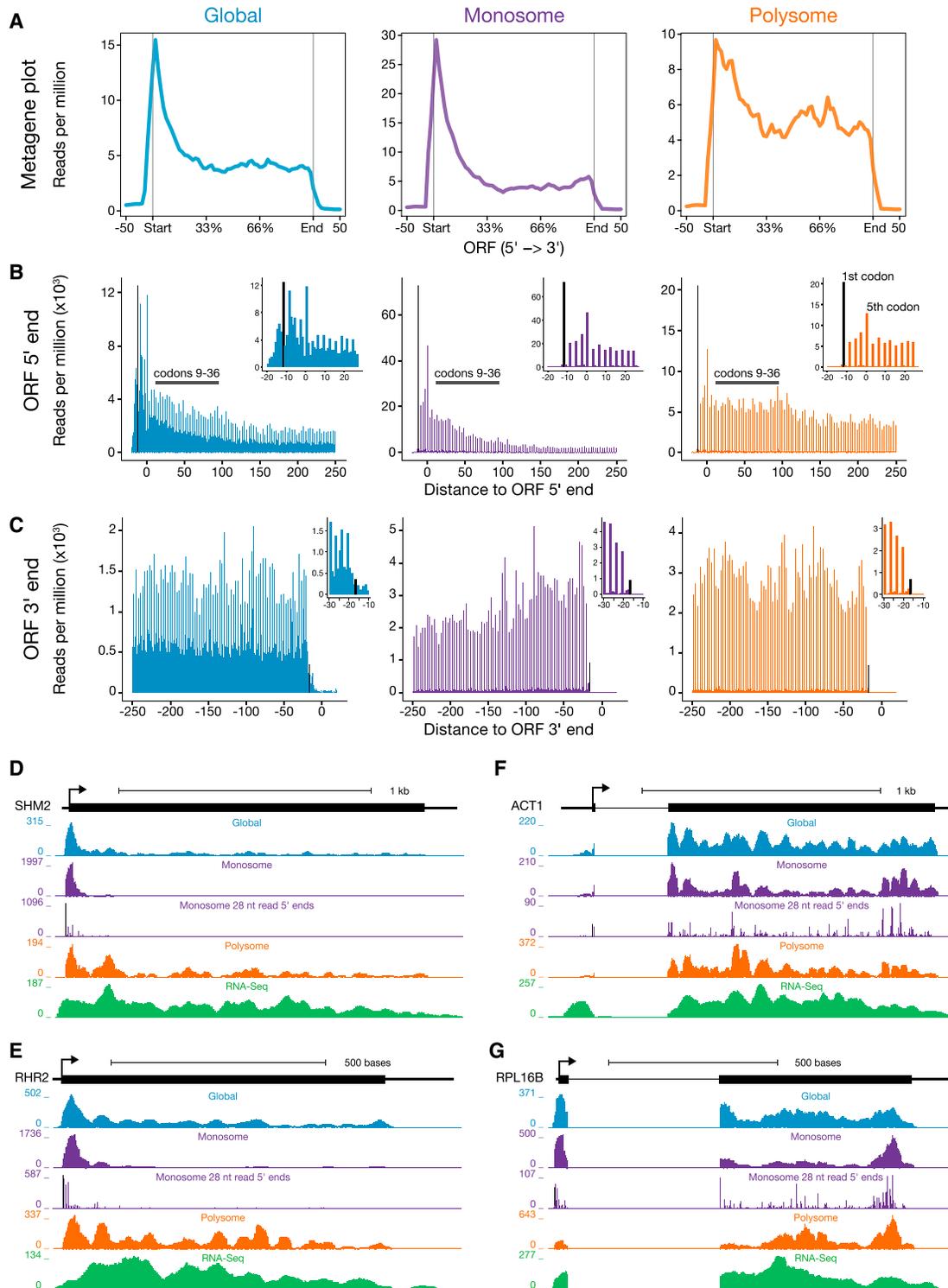
Figure 2. Global, Monosome, and Polysome Footprint Read Coverage

(A) Metagene plots using all ≥25 nt reads mapping to annotated genes.

(B) Aggregation plots using only 28-nt reads for all ORFs >300 nt. x axis: the distance from ORF 5′ end (i.e., first nucleotide of the start codon) to read 5′ end; y axis: reads per million (RPM). Gray bar indicates codons 9 to 36. Insets show first 13 codons (nt −20 to +27), with a peak at codon 1 indicated in black.

(C) Aggregation plots, as in (B), except distances are from ORF 3′ end (i.e., the third nucleotide of the stop codon) to read 5′ end. Insets show the last five codons (nt −30 to −10), with a 4-nt offset peak indicated in black.
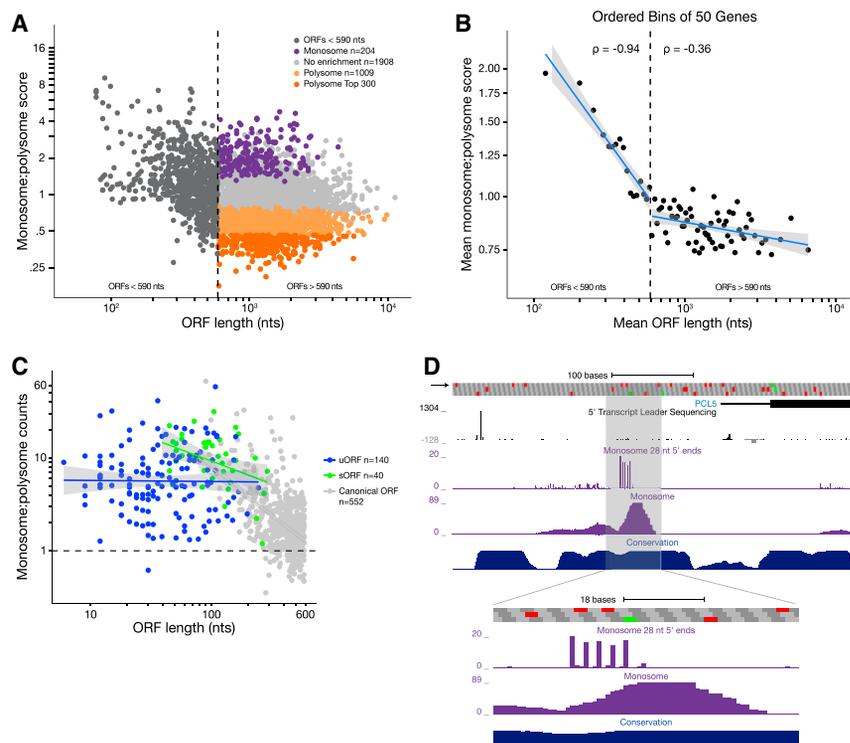
(legend continued on next page)

(A) Scatterplot of monosome:polysome score versus ORF length, with short ORF (dark gray dots), monosome (purple dots), polysome (orange dots), and no enrichment (light gray dots) sets indicated.

(B) Mean monosome:polysome score versus ORF length for ordered bins each containing 50 genes. Gray shading: 0.95 confidence interval; ρ: Pearson correlation coefficient.

(C) Scatterplot of monosome:polysome count ratio versus ORF length for canonical ORFs < 590 nt (gene; gray dots), sORFs (Smith et al., 2014; green dots), and uORFs (*Saccharomyces* Genome Database [SGD]-curated list from Ingolia et al., 2009; blue dots).

(D) Genome browser screenshot showing monosome footprint coverage and 3-nt phasing of 28-nt monosome footprints over a six-codon sORF upstream of PCL5. An arrow indicates the exon reading frame; green and red boxes indicate the start and stop codons, respectively. Conservation track represents evolutionary nucleotide conservation across seven *Saccharomyces* species.

See also Figure S3 and Tables S3 and S4.

uORF length. A likely explanation is that uORFs, by definition, are contained within multi-cistronic mRNAs whose cosedimentation with monosomes or polysomes is determined by the combined ribosome occupancy on all ORFs. Consequently, any simultaneous ribosome occupancy on multiple ORFs (even if each ORF is only occupied by a single ribosome) will cause the entire mRNA to cosediment with polysomes. Nonetheless, the strong bias of uORF ribosome footprints toward monosome cosedimentation indicates that when a ribosome is engaged on a uORF, all other ORFs in the mRNA tend to be unoccupied.

Because sORFs and uORFs are predominantly monosome associated, these regions had much higher occupancy in the monosome libraries than in either the polysome or global libraries. This enhanced detection suggested that monosome footprinting might prove more effective for identifying new sORFs than global ribosome footprinting, especially sORFs in monocistronic transcripts. To find new translationally active ORFs, we combined the two monosome libraries, removed reads associated with previously annotated ORFs (canonical, sORFs and uORFs), and then identified clusters of overlapping or adjacent genome-mapping reads in the remainder. Examination of high coverage clusters revealed that most occurred either within annotated 5′ UTRs or the region immediately upstream. One example is a uORF upstream of PCL5 (Figure 3D). Previ-

ously published 5′ transcript leader sequencing data (Arribere and Gilbert, 2013) suggests the existence of alternate transcription start sites (TSSs) for PCL5. Therefore, this uORF is likely an alternatively included element regulating PCL5 translation (Pelechano et al., 2013).

To identify features other than ORF length that affect the monosome:polysome score, we next considered only the 3,121 CDS genes with a canonical ORF >590 nt (Figure 3A). Within this set, DESeq2 identified 204 monosome-enriched (p-adj ≤ 0.001; Figure 3A, purple dots) and 1,009 polysome-enriched (p-adj ≤ 0.001; Figure 3A, orange dots) mRNAs (Table S3). To define the most extreme set of polysome-enriched mRNAs, we also picked the 300 mRNAs exhibiting the smallest monosome:polysome score (Figure 3A, dark orange dots). The remaining 1,908 mRNAs not meeting the above cutoffs formed the "no enrichment" set (p-adj > 0.001; Figure 3A, gray dots). We then compared various features of these four gene sets (Figure 4; data from this paper or previously published). Polysome-enriched genes have higher median mRNA and protein abundances than the no-enrichment and monosome-enriched sets (Figures 4A and 4F). Further, as is also expected for highly expressed genes, the polysome-enriched sets exhibit higher mRNA synthesis rates and longer mRNA half-lives than either the no-enrichment or monosome-enriched set (Figures 4B and

(D–G) Distribution of ≥25-nt reads from indicated libraries (solid plots) or 28-nt monosome 5′ read ends relative to the start codon (middle track) across individual genes. Whereas monosome reads on some genes predominate at the start codon (e.g., SHM2) or near the ORF 5′ end (e.g., RHR2), monosome reads on other genes (e.g., ACT1 and RPL16B) are spread throughout the entire ORF in a pattern similar to polysome and global footprints. All plots (A–G) were constructed from biological replicate 1 using only uniquely mapping reads.
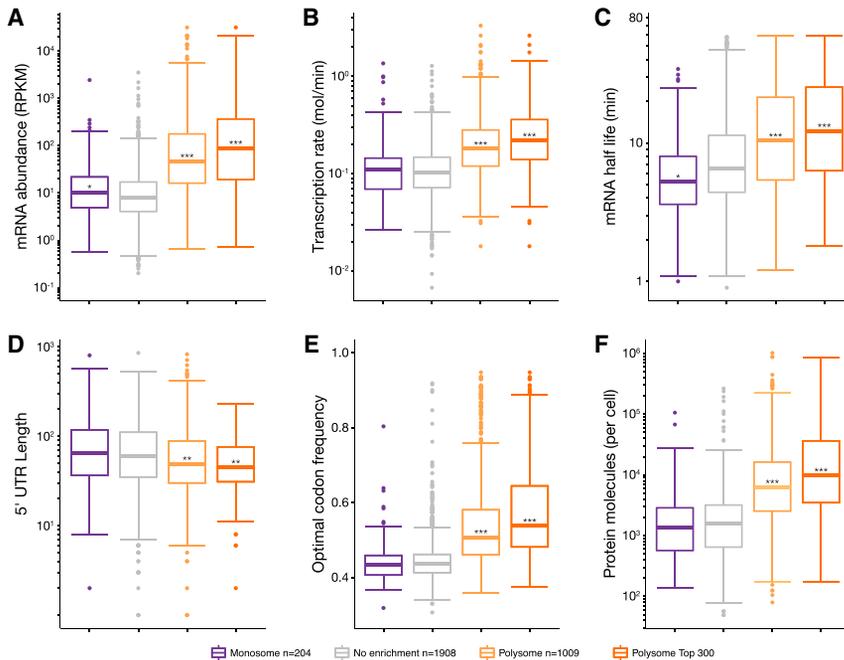
See also Figure S2 and Table S2.

tendency toward lower ribosome occupancy was also readily apparent in both a scatterplot of monosome versus polysome footprint RPKM (Figure 5C; quantified in Figures S4A and S4B) and boxplots of monosome:polysome scores (Figure 5C, inset). Unexpectedly, however, none of the three NMD target sets was statistically different from the non-NMD set with regard to mRNA half-life (Figure 5B). Thus, while NMD targets tend toward monosome occupancy, enrichment for NMD targets does not explain the lower median half-life of monosome-enriched mRNAs (Figure 4C). Consistent with this, the median half-life for monosome-enriched mRNAs remained significantly lower than the no enrichment set even when all known NMD targets were removed (Figure S4D). Thus, some feature other than NMD must be driving the lower stability of monosome-enriched mRNAs.

Ribosome Occupancy on Introns

Another set of known NMD targets are intron-containing transcripts that escape the nucleus without having been spliced (Sayani et al., 2008). Of 222 non-membrane genes harboring an intron inside the canonical ORF, 130 had ≥10 total monosome footprints that either partially or completely overlapped the intron. For these 130 introns, comparing the canonical ORF monosome:polysome score to the intron monosome:polysome count ratio revealed that ribosome footprints in introns were highly skewed toward monosomes, regardless of ORF monosome:polysome score (Figure 6A). Aggregation of 28-nt monosome footprint 5′ ends revealed strong exonic reading frame maintenance across the first 20 intronic codons (Figures 6B, 6C, and S5A). The sharp decrease in aggregated counts after the first few intron positions was due to the presence of an in-frame stop codon near the 5′ end of most introns. For genes with no early in-frame stop codon, phased monosome reads were readily observable within the intron (e.g, Figure 6E). In other introns, phased reads were also apparent on one or more internal sORFs on which ribosomes likely reinitiated after encountering the first stop codon (e.g., Figure 6F). The presence of such sORFs led to a decrease in phasing when all intron positions were taken into account (Figures 6D and S5B). Taken together, these data strongly support the idea that targeting of unspliced

4C). Finally, consistent with an evolutionary pressure toward more efficient translation, polysome-enriched mRNAs tend to have shorter 5′ UTRs (Figure 4D) and a higher optimal codon frequency (Figure 4E). In short, polysome-enriched mRNAs tend to be highly transcribed, have long mRNA half-lives, short 5′ UTRs, high codon optimality, and encode highly abundant proteins.

Monosomes, mRNA Half-Life, and NMD

In the above analysis, the monosome-enriched gene set had a lower median mRNA half-life than the no-enrichment set (Figure 4C; data from Presnyak et al., 2015). One class of mRNAs expected to be monosome enriched with shorter than average half-lives are those subject to nonsense-mediated mRNA decay (NMD). NMD preferentially eliminates transcripts wherein the stop codon exists in a suboptimal context for termination (Amrani et al., 2004), and NMD targeting is thought to occur when the first or "pioneer" ribosome encounters this suboptimal stop codon (Gao et al., 2005). Two previous studies independently identified two classes of genes in *S. cerevisiae* whose mRNA levels depend on NMD: (1) those with strong evidence of being "direct" NMD targets, and (2) those for which the evidence might indicate "indirect" regulation by NMD (Guan et al., 2006; Johansson et al., 2007). To facilitate our own comparative analysis, we parsed these partially overlapping gene sets according to whether both studies concurred on direct NMD target status (our class A; 33 non-membrane genes with ORF length >590 nt), a single study indicated direct NMD target status (class B; 144 genes), and any other gene indicated as an indirect target by either study (class C; 166 genes) (Table S3). All other genes were placed into a "non-NMD target" bin. Consistent with expectation, global ribosome footprint RPKM boxplots revealed that all three NMD target sets exhibited significantly lower overall ribosome occupancy than the non-NMD set (Figure 5A). This

A

Global footprint RPKM

B

mRNA half life (mins)

C

Monosome footprint (RPKM)

Polysome footprint (RPKM)

Class A n=33
Class B n=144
Class C n=166
Remainder n=2778
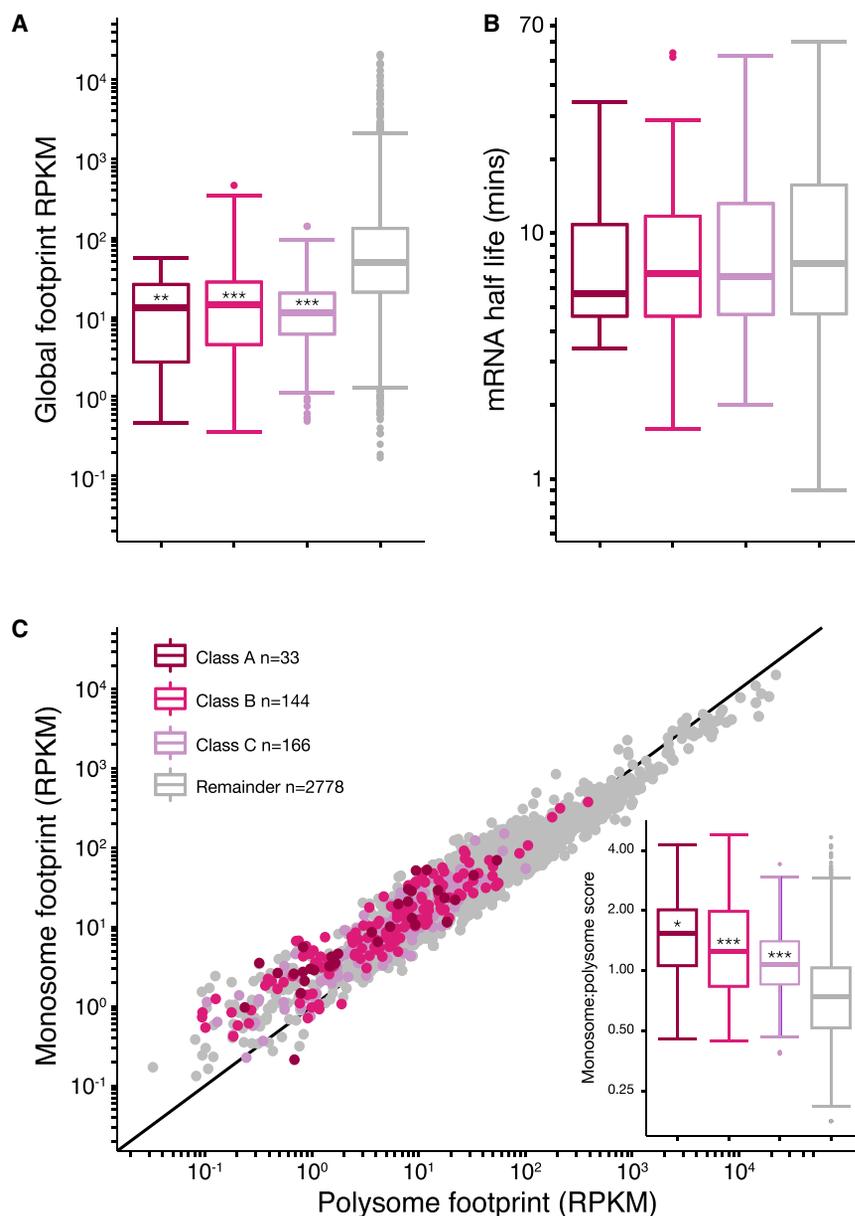
Monosome:polysome score

Figure 5. Characteristics of NMD-Regulated Genes

(A and B) Boxplots comparing mean global footprint RPKM (A) and mRNA half-life (B; Presnyak et al., 2015) for classes of direct and indirect NMD targets (Guan et al., 2006; Johansson et al., 2007) as indicated in (C).

(C) Scatterplot comparing mean monosome and polysome footprint RPKM for indicated gene sets. Inset: boxplots of monosome:polysome scores for the same gene sets. ***p < 2.2 × 10^{-16}; **p = 6.1 × 10^{-11}; *p = 2.0 × 10^{-10}; all others p > 0.05; Wilcoxon rank-sum test compared to "Remainder." See also Figure S4.

population), mRNAs encoding kinases and transcription regulators were overrepresented in the 204-member monosome-enriched set (Table S4). Such regulatory proteins tend to be required in low copy numbers per cell. Notably, both overall ribosome density and calculated protein output were substantially lower for our monosome-enriched genes than all other gene sets (Figures S6A and S6B). Many mRNAs encoding regulatory proteins are also subject to negative translation regulation (e.g., by uORFs; see below). Consistent with this, canonical ORFs downstream of a uORF exhibited greater monosome enrichment than canonical ORFs not preceded by any annotated uORF (Figure S6D). Thus, long ORF mRNAs typically occupied by single ribosomes tend to encode low-abundance proteins and be subject to negative translation regulation.

By integrating fixed parameters, such as average cell size and ribosome abundance, with numerous transcriptome-wide datasets (e.g., RNA-seq, RiboSeq, mRNA half-life, and tRNA decoding specificity), Siwiak and Zielenkiewicz (2010) recently established a quantitative, computational model of translation in *S. cerevisiae* from which various statistics (e.g., initiation time, time required to form a new 80S ribosome at the start codon; total elongation time, time required for a ribosome to elongate through the entire ORF) were calculated for each mRNA (Siwiak and Zielenkiewicz, 2010). In theory, the number of ribosomes occupying an mRNA should be a function of initiation time versus total elongation time. If initiation time is considerably longer than total elongation time, then an mRNA should on average be occupied by zero or one ribosome, but rarely by two or more. Consistent with this, the ratio of initiation time to total elongation time was highest for our two monosome-enriched populations (i.e., the ORF <590-nt and ORF >590-nt monosome-enriched sets) compared to all other gene sets (Figure 7C). For the ORF <590-nt set, the major driver of this ratio was short

transcripts for NMD occurs predominantly on monosomes. They further demonstrate that introns can harbor translationally active sORFs, so may represent a previously unrecognized source of short peptide translation products. As with other sORFs, ribosome occupancy on intronic sORFs was only readily detectable in the monosome and not polysome or global libraries. This again highlights the usefulness of monosome footprinting for detecting low-density ribosome occupancy.

Initiation and Elongation Times Determine Monosome Association

For genes with canonical ORFs long enough to accommodate more than one ribosome, why are some still predominantly monosome associated? Compared to all 3,121 cytoplasmic CDS genes with canonical ORFs > 590 nt (i.e., our background
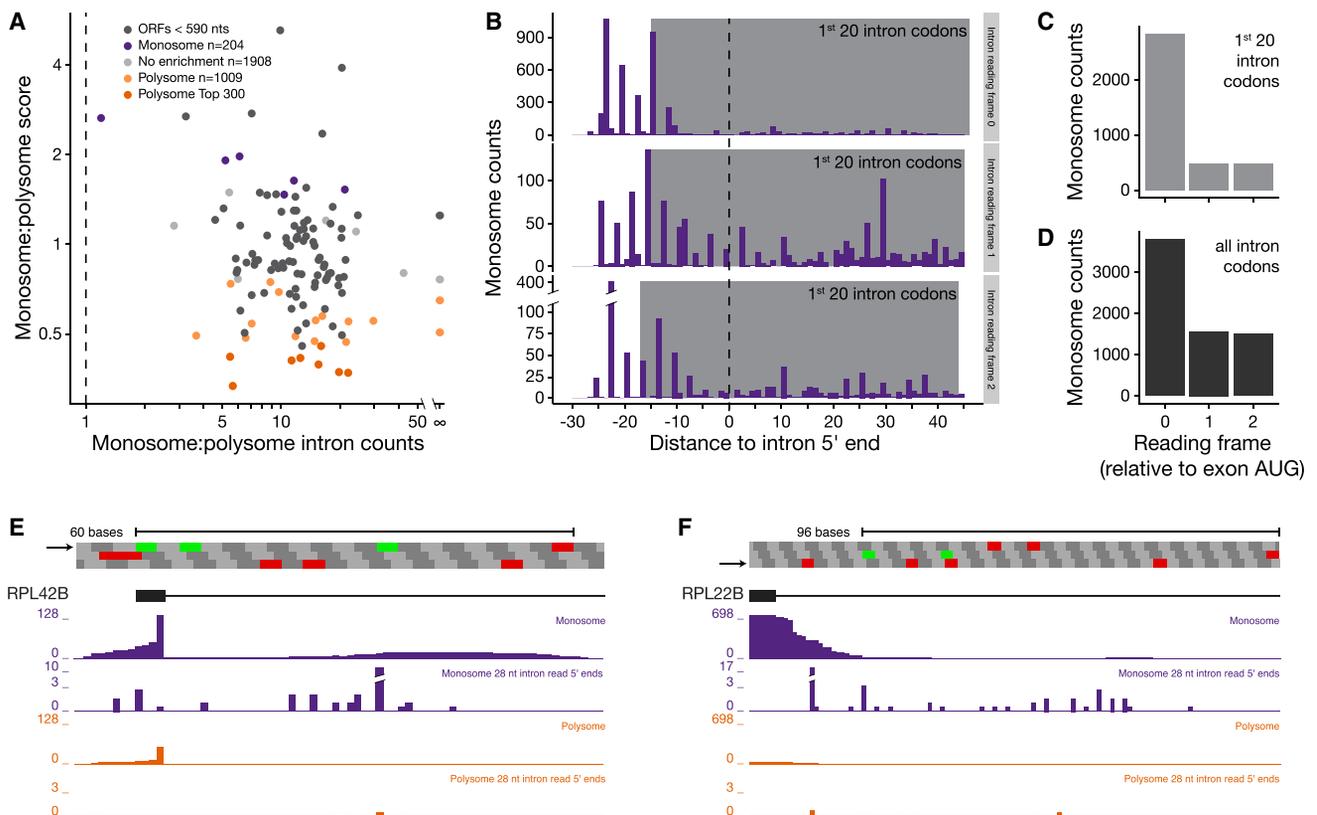
Figure 6. Monosome Footprints on Introns

(A) Scatterplot showing ORF monosome:polysome score versus intronic monosome:polysome footprint ratio for intron-containing members of the gene sets defined in Figure 3A.

(B) Aggregation plots combining both monosome biological replicates of 28-nt reads overlapping the first intron by ≥1 nt. x axis: intron 5′ end to read 5′ end distance; y axis: read count; gray boxes: 5′ read end positions indicative of ribosomal A-site occupancy by intronic codons 1–20.

(C and D) Bar charts quantifying reading frame use across intronic codons 1–20 (C; region highlighted by gray boxes in B) or across the entire intron (D).

(E and F) Distribution of ≥25 nt reads from indicated libraries (solid plots) or 5′ ends of 28-nt intronic reads across individual genes. Plots were constructed from biological replicate 1 using only uniquely mapping reads. An arrow indicates exon reading frame; green and red boxes indicate start and stop codons, respectively.

See also Figure S5.

total elongation time (Figure 7B) due to ORF length. Conversely, for the >590-nt monosome-enriched set, the major driver was initiation time (Figure 7A). Thus, many long ORFs tend toward monosome occupancy due to slow initiation rates.

The relationship between initiation and elongation times also leads to different monosome and polysome footprint patterns across individual genes (Figures 7D and 7F). For mRNAs in which initiation time is substantially slower than total elongation time, any ribosome occupying that mRNA will generally be in the process of elongation. It follows that mRNAs with extremely slow initiation rates should be predominantly monosome associated, with ribosome footprints distributed across the entire ORF (Figure 7F, class I). One example is BER1, a regulator of microtubule stability involved in proper kinetochore function (Fiechter et al., 2008). Another is GCN4, a highly studied transcription factor required for upregulation of amino acid biosynthesis upon starvation. Initiation on the canonical GCN4 ORF is regulated by four uORFs; translation across a uORF generally decreases downstream re-initiation efficiency (Hinnebusch, 2005). The

very high enrichment of all four GCN4 uORFs in the monosome libraries (monosome:polysome counts = 9.0, 8.3, 10.5, and 6.1, respectively; Figure S6F) indicates a strong preference for only one GCN4 ORF (one uORF or the canonical ORF) to be occupied at a time. Consistent with this, the canonical ORF exhibited strong monosome enrichment (monosome:polysome counts = 3.7), with footprints distributed throughout its entire length (Figure 7F, class I). Therefore, the rate-limiting step for GCN4 translation during logarithmic growth in rich media is initiation on the canonical ORF.

Other mRNAs primarily occupied by monosomes are those on which a newly initiated 80S lingers for an extended time either at the start codon (i.e., the transition from initiation into elongation is extremely slow) or immediately downstream (i.e., elongation through codons 2–9 is extremely slow) (Figures 2D and 7F, class II). While the possibility of new initiation events occurring during sample workup always warrants cautious interpretation of reads at ORF 5′ ends (Gerashchenko and Gladyshev, 2014), any ribosome occupancy at the beginning of the ORF necessarily
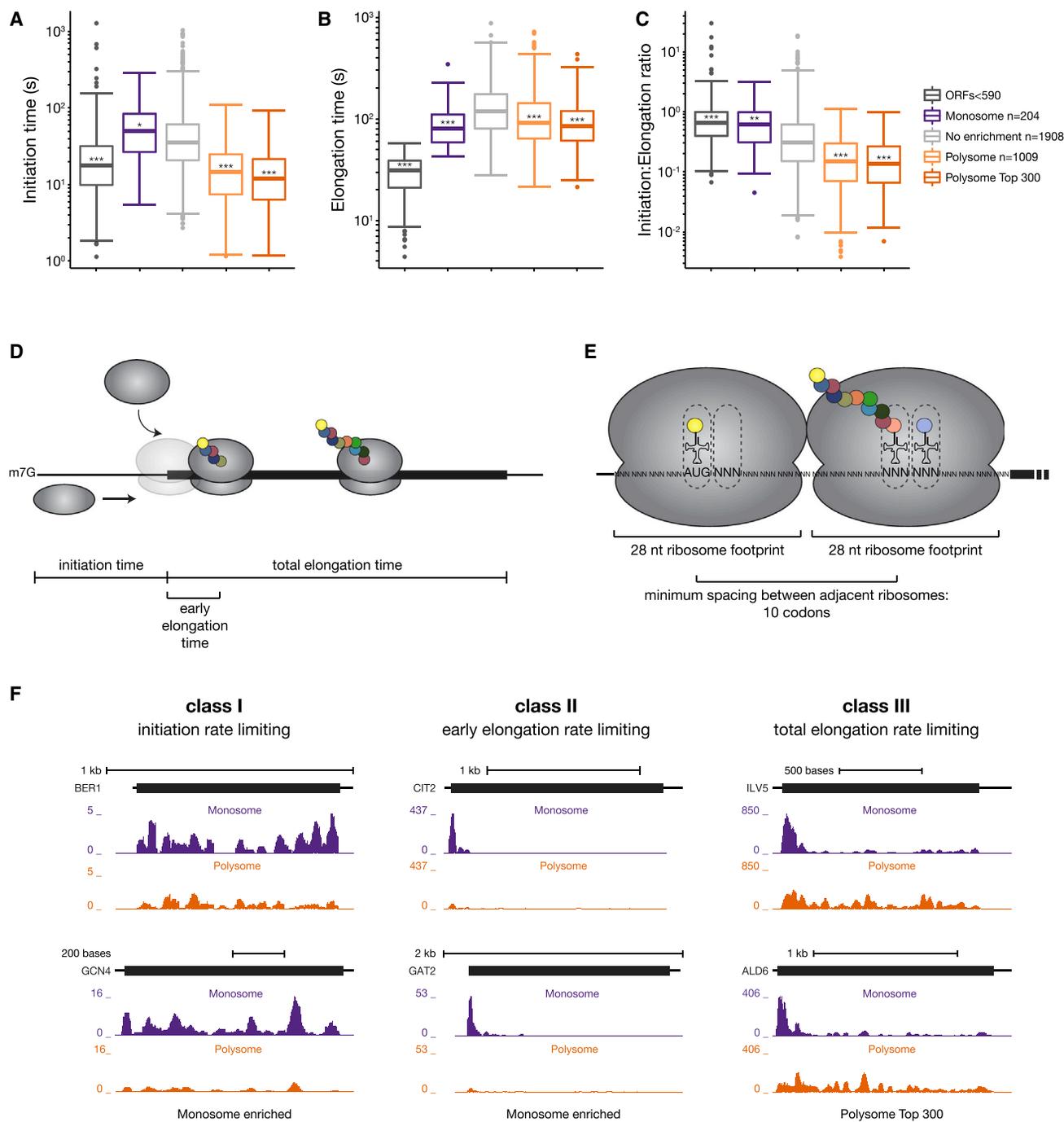
Figure 7. Relationship between Initiation and Elongation Times Determines Degree of Monosome versus Polysome Association

(A–C) Boxplots comparing initiation time (A), elongation time (B), or the ratio of initiation:elongation time (C) for the gene sets defined in Figure 3A; data are from Siwiak and Zielenkiewicz (2010). ***p < 2.2 × 10^{-16}; **p = 7.5 × 10^{-15}; *p = 5.2 × 10^{-5}; all others p > 0.05; Wilcoxon rank-sum test compared to "No enrichment."

(D) Schematic showing the relative position of ribosomes and individual subunits during initiation, early elongation, and total elongation. Opaque ribosome over start codon indicates block to 80S formation while another ribosome occupies the region immediately downstream of the start codon.

(E) Schematic showing minimum spacing between adjacent ribosomes.

(F) Distribution of ≥25-nt reads from monosome and polysome libraries across genes representative of classes discussed in text.

See also Figure S6.

prevents a second ribosome from assembling over the start codon due to steric hindrance (see Figure 7E, schematic). The footprint pattern expected for class II genes is high monosome signal limited to the very beginning of the ORF, combined with low polysome signal wherein the footprint distribution exhibits a strong peak akin to the monosome peak at the beginning of the ORF and low, but even, coverage across the remainder.

Examples of class II genes were readily apparent in the 204-member monosome-enriched set. For SHM2, most of the monosome reads occurred immediately over the start codon, with the remainder of the ORF only occupied in polysomes (Figure 2D). The reason for AUG stalling on SHM2 mRNA may be the highly suboptimal CCU proline codon (Artieri and Fraser, 2014; Gardin et al., 2014) at position 2. Regardless of the cause, the transition from initiation to elongation is clearly rate limiting for SHM2 translation in logarithmically growing yeast. CIT2 and GAT2 are paradigmatic examples of mRNAs for which elongation through codons 2–9 is rate limiting for overall translation (Figure 7F, class II). For both, monosome footprints were confined to the beginning of the ORF, with the rest of the ORF only exhibiting low ribosome occupancy in the polysome libraries. Slow transit at the beginning of an ORF might be due to highly suboptimal codons in this region. It should be noted, however, that suboptimal codons tend to be enriched at ORF 5′ ends transcriptome-wide (Tuller et al., 2010), and when we calculated optimal codon frequency and codon adaptation index across codons 2–9, we found no statistically significant difference between class II genes and any other gene set (data not shown). Consequently, we currently have no clear explanation for slow ribosome transit across codons 2–9 in class II genes, though codon arrangement could certainly play a role (Ciandrini et al., 2013).

At the opposite end of the spectrum with regard to initiation rate are genes encoding high-abundance proteins (Figure 7F, class III). Both the 1,009-member and top-300 polysome-enriched sets with ORFs > 590 nt (Figure 3A) are highly enriched in mRNAs encoding proteins involved in translation, RNP biogenesis, and general metabolism (e.g., amino acid biosynthesis, glycolysis) (Table S4). Because each mRNA molecule must turn out massive amounts of protein during logarithmic growth (Figure S6B), these genes have the shortest initiation times (Figure 7A) and the highest elongation rates (i.e., codons per second; Figure S6C). Their translation is limited only by the time required to complete elongation (Figure 7B). Therefore, the paradigmatic footprint pattern for this class is high and uniform density across the ORF in the polysome libraries, with monosome reads predominating at ORF 5′ ends (Figure 7F, class III). For such highly translated genes (as exemplified by mRNAs encoding ribosomal proteins; Figure S6E), their relative association with monosomes or polysomes is almost entirely a function of ORF length.

In summary, the above results clearly demonstrate that the ratio of total time required to complete initiation and liberate the start codon for occupancy by another ribosome versus total time required to complete elongation is a major factor determining polysome versus monosome association. Whereas mRNAs with long ORFs and high initiation rates tend to be translated primarily on polysomes, mRNAs with short ORFs and/or slow initiation rates are predominately occupied by monosomes.

DISCUSSION

In this paper, we examined the translational status of 80S monosomes in *S. cerevisiae*. Countering the widespread notion that translationally active mRNAs are limited to polysomes, we found ample evidence for translation elongation by monosomes. Strong 3-nt phasing of monosome footprints at both the 5′ and 3′ ends of ORFs in transcriptome-wide aggregation plots indicates that monosomes can both initiate and complete elongation. Indeed, the vast majority of monosome footprints were located downstream of the start codon, and 75% of canonical ORFs exhibited internal monosome occupancy. Thus, for most mRNA species, some fraction of molecules is occupied by a single, translationally active ribosome. For species with short ORFs or slow initiation rates, the majority of mRNA molecules are monosome-associated. Monosomes also predominate on NMD targets, unspliced pre-mRNAs and mRNAs encoding low abundance regulatory proteins. Therefore, the 80S monosome fraction should no longer be viewed as translationally inactive. Rather, monosomes are key contributors to the overall cellular translatome.

The First Round of Translation and Translational Ramps
When aggregated across all genes, global ribosome footprints tend to peak at ORF 5′ ends, sharply decrease across the first 30–40 codons and then gradually reach a plateau that persists throughout the remainder of the ORF (Ingolia et al., 2009). This pattern has been proposed to reflect an evolutionarily conserved "translational ramp," a region containing suboptimal codons through which newly initiated ribosomes elongate slowly before speeding up to maximal efficiency within the ORF body, presumably to minimize ribosome traffic jams and thereby the energetic cost of protein synthesis (Tuller et al., 2010). Our data do not support the translational ramp hypothesis. If all newly initiated ribosomes first proceed slowly, the same sharp footprint drop-off at ORF 5′ ends should occur regardless of whether or not the mRNA is concurrently occupied by other ribosomes. However, our polysome and monosome libraries displayed quite different profiles, with polysomes almost completely lacking a ramp and monosomes having an even more pronounced ramp than the global libraries (Figures 2B, S2A, S2C, and S2D). We conclude that the observed global ramp is almost entirely due to the monosome component.

Why do monosome aggregation plots display such a steep ramp at the beginning of the ORF? When any mRNA transitions from the free mRNP pool to the translationally active pool, the first several codons must necessarily be translated by a monosome. This is because a second ribosome cannot form at the start codon until the first has moved sufficiently far into the ORF that it no longer sterically blocks a second from assembling (Figure 7E). Based on the known lengths of ribosome footprints, 10 codons is the minimum spacing between the first elongating ribosome and a second at the AUG (i.e., codon 11 in the P site of the first ribosome and the AUG in the P site of the second ribosome). Upon assembly of the second ribosome, the mRNA becomes a polysome, so is thereby removed from the monosome pool. The dramatic decrease starting after codon 9 in the transcriptome-wide monosome aggregation plots fully supports

this minimum spacing (Figures 2B, S2A, S2C, and S2D). This pattern was also clearly present on individual mRNAs (Figures 2E and 7F, class II). We therefore conclude that the apparent "translational ramp" in global footprint aggregation plots is simply due to steric constraints on assembly of multiple ribosomes at the 5′ ends of ORFs.

Monosomes, NMD Targets, and mRNA Half-Lives

Nonsense-mediated mRNA decay (NMD) is a cellular process that both degrades aberrant mRNAs containing premature termination codons and regulates a subset of wild-type mRNAs (He et al., 2003). It has been proposed that NMD occurs predominantly as a consequence of the first round of translation (Culbertson and Neeno-Eckwall, 2005; Gao et al., 2005). If so, NMD substrates should exhibit lower than average overall ribosome occupancy in global footprinting experiments and be predominantly monosome-associated. Both expectations proved valid for three non-overlapping sets of previously identified NMD targets (Figures 5B and 5C, inset). Surprisingly, however, no NMD target set was statistically different from the non-NMD set with regard to mRNA half-life (Figure 5A). Consequently, a predominance of NMD targets cannot explain the lower median mRNA half-life of the 204-member monosome-enriched gene set compared to the no-enrichment set (Figure 3C). Consistent with this, removal of all NMD targets only negligibly affected median half-lives of the monosome-enriched, no-enrichment and polysome-enriched gene sets (Figures S4C and S4D), with the difference between the monosome-enriched and no-enrichment median half-lives still being highly significant (p = 0.001). So why do monosome-enriched mRNAs have shorter half-lives? Overall codon optimality was recently shown to be the major determinant of mRNA half-life in *S. cerevisiae* (Presnyak et al., 2015). However, even with the NMD targets removed, we found no statistically significant difference between the monosome-enriched and no-enrichment sets with regard to codon optimality (Figures S4E and S4F). In the end, while our data do indicate a relationship between mRNA half-life and monosome occupancy, we have yet to find a mechanistic explanation.

Monosomes, sORFs, and Biologically Active Peptides

Recent work across diverse organisms has discovered the existence of thousands of biologically active peptides synthesized directly from sORFs rather than being proteolytically cleaved from larger precursors (for reviews, see Storz et al., 2014; Chu et al., 2015; Landry et al., 2015). If we are to understand the complete repertoire of such peptides, new methods for identifying translationally active sORFs are required. Two recent studies expressly sought to accomplish this by ribosome profiling (Aspden et al., 2014; Smith et al., 2014). Because both analyses were limited to transcripts cosedimenting with polysomes, however, only those sORFs long enough to accommodate two or more ribosomes could be interrogated. Not surprisingly, our datasets reveal a very strong relationship between ORF length and monosome:polysome score, with the shortest canonical ORFs being highly monosome enriched (Figures 3A and 3B). This same trend exists for the *S. cerevisiae* sORFs identified above (Smith et al., 2014; Figure 3C), suggesting that identification of new sORFs is better accomplished by monosome profiling.

Our own datasets have already revealed a conserved uORF upstream of the canonical PCL5 ORF (Figure 3D), as well as several translationally active sORFs in introns (e.g., Figure 6F). Thus, monosome profiling is a highly effective method for expanding the universe of sORFs that serve either as translational regulators (e.g., uORFs) and/or sources of new biologically active peptides.

Monosome Association: A Function of Initiation versus Elongation

In addition to transcripts with sORFs and uORFs, scores of mRNAs with canonical ORFs were highly enriched in the monosome fraction. Some encode high abundance species, such as ribosomal proteins (RPs). Because RPs are constantly required to produce new ribosomes during logarithmic growth, RP mRNAs are among the most efficiently translated of all mRNAs. The two shortest RP ORFs are both 78 nt and encode RPL41A and B. Based on the number of ribosomes per cell and *S. cerevisiae* doubling time in rich media, Yu and Warner (2001) estimated that initiation and completion of RPL41A/B translation requires only ~2 s. If the combined rates of elongation and termination are faster than initiation, then, at steady state, the preponderance of short, highly translated mRNAs should be associated with just a single ribosome. Consistently, both RPL41 mRNAs were previously shown to be predominantly monosome associated (Yu and Warner, 2001), and they were among the most highly monosome-enriched canonical ORF transcripts in our datasets (Figure 3A).

RPL41A and B illustrate the general principle that any mRNA will be predominantly monosome associated if the combined time required for elongation and termination is much shorter than the time required for initiation. Because total elongation time strongly depends on ORF length (Siwiak and Zielenkiewicz, 2010), the monosome:polysome score should be a function of ORF length up to the point at which the elongation phase is of similar duration as the initiation phase. This likely explains the steep slope and tight correlation between mean/median monosome:polysome score and ORF length up to 590 nt (Figures 3B and S3F). Beyond this inflection point, most mRNAs are predominantly polysome associated because the elongation phase is now longer than the initiation phase. Nonetheless, even among mRNAs with ORFs > 590 nt, many remained predominantly monosome associated (our 204-member monosome gene set; Figure 3A). This set has significantly longer initiation times than all other gene sets (Figure 7A), driving the initiation:elongation ratio to be comparable to the ORF <590-nt gene set (Figure 7C). Therefore, mRNAs with very long initiation times are predominantly monosome associated. Included among mRNAs with long initiation times are those subject to negative translation regulation and those encoding low-abundance regulatory proteins.

Perspective

The long-standing assumption that all translation occurs on polysomes, and therefore that 80S monosomes are translationally inactive, has had important ramifications in multiple biological systems. For instance, studies that focus solely on mRNAs cosedimenting with polysomes (e.g, Aspden et al., 2014; Krishnan et al., 2014; Reboll and Nourbakhsh, 2014; Smith

et al., 2014) will severely underestimate translational flux for mRNAs on which initiation is significantly slower than elongation and termination. These include mRNAs with sORFs, mRNAs with long and highly structured 5′ UTRs, and mRNAs on which translation initiation is subject to negative regulation under the particular cellular conditions being examined. Pre-selection of polysomes also eliminates the possibility of identifying sORFs that are only long enough to accommodate a single ribosome.

The ''polysome-only'' assumption has also served as a strong and long-standing argument against localized translation in mature mammalian axons, where visible polysomes are generally lacking (Holt and Schuman, 2013; Steward and Schuman, 2003). Even in dendrites, where localized translation is well established, the polysome-only assumption leads to large discrepancies between biochemical measurements of translation and the amount of translation theoretically possible based only on visible polysome numbers per dendritic spine (Ostroff et al., 2002). Our finding that mRNAs encoding key regulatory factors and other low-abundance proteins are predominantly translated by monosomes in *S. cerevisiae* opens the possibility that monosomes are also active in neuronal processes, where many polypeptides required for modulating synaptic strength are required at low stoichiometries per synapse (Sheng and Hoogenraad, 2007; Sheng and Kim, 2011). At least one of these synaptic modulators, Arc/Arg3.1, is a natural NMD target (Bicknell et al., 2012; Giorgi et al., 2007), and so may be preferentially monosome-associated as are *S. cerevisiae* NMD targets (Figure 5C, inset).

EXPERIMENTAL PROCEDURES

See the Extended Experimental Procedures for additional Experimental Procedures.

Ribosome Footprinting

BY4741 yeast were grown in YEPD, harvested at optical density 600 0.6 after a 2-min cycloheximide treatment, and lysed by vortexing with glass beads. For global ribosome footprinting, 50 A_{260} units of clarified lysate were digested with RNase I and separated through a 35-ml 6%–38% sucrose gradient. 80S monosome fractions were collected and RNA extracted. For monosome or polysome footprinting, clarified lysate was separated through a 35 ml 6%–38% gradient. Fractions corresponding to either monosomes or polysomes were collected separately; each was diluted in an equal volume of gradient buffer and concentrated. Post-concentration, 2 A_{260} units of each sample were digested with RNase I and separated through a 10.5-ml 10%–50% sucrose gradient. 80S fractions were collected, and the RNA was extracted following the same procedure as for global footprints.

RNA-Seq and Library Preparation

5 μg of total RNA from clarified lysate was depleted of rRNA prior to fragmentation and size selection. RNA fragments (∼20–45 nt) were isolated by denaturing PAGE for RNA-seq; ribosome footprints (27–31 nt) were isolated in a similar manner. All RNA fragments were converted into deep-sequencing libraries using a modified version of our standard laboratory protocol (Heyer et al., 2015). Briefly, a preadenylated adaptor was ligated to RNA 3′ ends, after which time the ligated RNAs were reverse transcribed. The RT product is gel purified, circularized, and PCR amplified prior to sequencing.

Mapping and Analysis of Deep-Sequencing Data

Barcoded libraries were pooled and sequenced on either an Illumina Hi-Seq2000 (ribosome footprints) or MiSeq (RNA-seq). Reads were parsed into appropriate libraries by 5′ barcode, and then adaptor sequences were removed. Trimmed reads were filtered for non-coding RNAs, and the remaining reads were mapped to both the sacCer3 genome (in a splice-aware fashion) and transcriptome, with the former being viewed on the UCSC genome browser. Uniquely mapping reads ≥25 nt (ribosome footprints) or ≥22 nt (RNA-seq) were used for all analyses unless otherwise indicated. Data analyses were performed using the R software package.

ACCESSION NUMBERS

The accession number for the sequencing data reported in this paper has been uploaded to NCBI's GEO: GSE76117.

SUPPLEMENTAL INFORMATION

Supplemental Information includes Supplemental Experimental Procedures, six figures, and four tables and can be found with this article online at http://dx.doi.org/10.1016/j.cell.2016.01.003.

AUTHOR CONTRIBUTIONS

E.E.H. and M.J.M. conceived of the experiments and wrote the manuscript. E.E.H. conducted all experiments and bioinformatic analysis.

ACKNOWLEDGMENTS

REFERENCES

Amrani, N., Ganesan, R., Kervestin, S., Mangus, D.A., Ghosh, S., and Jacobson, A. (2004). A faux 3′-UTR promotes aberrant termination and triggers nonsense-mediated mRNA decay. Nature *432*, 112–118.

Arava, Y., Wang, Y., Storey, J.D., Liu, C.L., Brown, P.O., and Herschlag, D. (2003). Genome-wide analysis of mRNA translation profiles in Saccharomyces cerevisiae. Proc. Natl. Acad. Sci. USA *100*, 3889–3894.

Arribere, J.A., and Gilbert, W.V. (2013). Roles for transcript leaders in translation and mRNA decay revealed by transcript leader sequencing. Genome Res. *23*, 977–987.

Artieri, C.G., and Fraser, H.B. (2014). Accounting for biases in riboprofiling data indicates a major role for proline in stalling translation. Genome Res. *24*, 2011–2021.

Aspden, J.L., Eyre-Walker, Y.C., Phillips, R.J., Amin, U., Mumtaz, M.A.S., Brocard, M., and Couso, J.-P. (2014). Extensive translation of small open reading frames revealed by poly-ribo-seq. eLife *3*, e03528.

Bhattacharya, A., McIntosh, K.B., Willis, I.M., and Warner, J.R. (2010). Why Dom34 stimulates growth of cells with defects of 40S ribosomal subunit biosynthesis. Mol. Cell. Biol. *30*, 5562–5571.

Bicknell, A.A., Cenik, C., Chua, H.N., Roth, F.P., and Moore, M.J. (2012). Introns in UTRs: why we should stop ignoring them. BioEssays *34*, 1025–1034.

Brown, A., Shao, S., Murray, J., Hegde, R.S., and Ramakrishnan, V. (2015). Structural basis for stop codon recognition in eukaryotes. Nature *524*, 493–496.

Chu, Q., Ma, J., and Saghatelian, A. (2015). Identification and characterization of sORF-encoded polypeptides. Crit. Rev. Biochem. Mol. Biol. *50*, 134–141.

Ciandrini, L., Stansfield, I., and Romano, M.C. (2013). Ribosome traffic on mRNAs maps to gene ontology: genome-wide quantification of translation initiation rates and polysome size regulation. PLoS Comput. Biol. 9, e1002866.

Culbertson, M.R., and Neeno-Eckwall, E. (2005). Transcript selection and the recruitment of mRNA decay factors for NMD in Saccharomyces cerevisiae. RNA 11, 1333–1339.

Favaudon, V., and Pochon, F. (1976). Magnesium dependence of the association kinetics of Escherichia coli ribosomal subunits. Biochemistry 15, 3903–3912.

Fiechter, V., Cameroni, E., Cerutti, L., De Virgilio, C., Barral, Y., and Fankhauser, C. (2008). The evolutionary conserved BER1 gene is involved in microtubule stability in yeast. Curr. Genet. 53, 107–115.

Gao, Q., Das, B., Sherman, F., and Maquat, L.E. (2005). Cap-binding protein 1-mediated and eukaryotic translation initiation factor 4E-mediated pioneer rounds of translation in yeast. Proc. Natl. Acad. Sci. USA 102, 4258–4263.

Gardin, J., Yeasmin, R., Yurovsky, A., Cai, Y., Skiena, S., and Futcher, B. (2014). Measurement of average decoding rates of the 61 sense codons in vivo. eLife 3, e03735.

Gerashchenko, M.V., and Gladyshev, V.N. (2014). Translation inhibitors cause abnormalities in ribosome profiling experiments. Nucleic Acids Res. 42, e134.

Ghaemmaghami, S., Huh, W.-K., Bower, K., Howson, R.W., Belle, A., Dephoure, N., O'Shea, E.K., and Weissman, J.S. (2003). Global analysis of protein expression in yeast. Nature 425, 737–741.

Giorgi, C., Yeo, G.W., Stone, M.E., Katz, D.B., Burge, C., Turrigiano, G., and Moore, M.J. (2007). The EJC factor eIF4AIII modulates synaptic strength and neuronal protein expression. Cell 130, 179–191.

Guan, Q., Zheng, W., Tang, S., Liu, X., Zinkel, R.A., Tsui, K.-W., Yandell, B.S., and Culbertson, M.R. (2006). Impact of nonsense-mediated mRNA decay on the global expression profile of budding yeast. PLoS Genet. 2, e203.

Guydosh, N.R., and Green, R. (2014). Dom34 rescues ribosomes in 3′ untranslated regions. Cell 156, 950–962.

Han, Y., Gao, X., Liu, B., Wan, J., Zhang, X., and Qian, S.-B. (2014). Ribosome profiling reveals sequence-independent post-initiation pausing as a signature of translation. Cell Res. 24, 842–851.

He, F., Li, X., Spatrick, P., Casillo, R., Dong, S., and Jacobson, A. (2003). Genome-wide analysis of mRNAs regulated by the nonsense-mediated and 5′ to 3′ mRNA decay pathways in yeast. Mol. Cell 12, 1439–1452.

Heyer, E.E., Özadam, H., Ricci, E.P., Cenik, C., and Moore, M.J. (2015). An optimized kit-free method for making strand-specific deep sequencing libraries from RNA fragments. Nucleic Acids Res. 43, e2.

Hinnebusch, A.G. (2005). Translational regulation of GCN4 and the general amino acid control of yeast. Annu. Rev. Microbiol. 59, 407–450.

Holt, C.E., and Schuman, E.M. (2013). The central dogma decentralized: new perspectives on RNA function and local translation in neurons. Neuron 80, 648–657.

Ingolia, N.T., Ghaemmaghami, S., Newman, J.R.S., and Weissman, J.S. (2009). Genome-wide analysis in vivo of translation with nucleotide resolution using ribosome profiling. Science 324, 218–223.

Ingolia, N.T., Brar, G.A., Stern-Ginossar, N., Harris, M.S., Talhouarne, G.J.S., Jackson, S.E., Wills, M.R., and Weissman, J.S. (2014). Ribosome profiling reveals pervasive translation outside of annotated protein-coding genes. Cell Rep. 8, 1365–1379.

Johansson, M.J.O., He, F., Spatrick, P., Li, C., and Jacobson, A. (2007). Association of yeast Upf1p with direct substrates of the NMD pathway. Proc. Natl. Acad. Sci. USA 104, 20872–20877.

Krishnan, K., Ren, Z., Losada, L., Nierman, W.C., Lu, L.J., and Askew, D.S. (2014). Polysome profiling reveals broad translatome remodeling during endoplasmic reticulum (ER) stress in the pathogenic fungus Aspergillus fumigatus. BMC Genomics 15, 159.

Landry, C.R., Zhong, X., Nielly-Thibault, L., and Roucou, X. (2015). Found in translation: functions and evolution of a recently discovered alternative proteome. Curr. Opin. Struct. Biol. 32, 74–80.

Love, M.I., Huber, W., and Anders, S. (2014). Moderated estimation of fold change and dispersion for RNA-seq data with DESeq2. Genome Biol. 15, 550.

Nagalakshmi, U., Wang, Z., Waern, K., Shou, C., Raha, D., Gerstein, M., and Snyder, M. (2008). The transcriptional landscape of the yeast genome defined by RNA sequencing. Science 320, 1344–1349.

Noll, H. (2008). The discovery of polyribosomes. BioEssays 30, 1220–1234.

Noll, M., Hapke, B., Schreier, M.H., and Noll, H. (1973). Structural dynamics of bacterial ribosomes. I. Characterization of vacant couples and their relation to complexed ribosomes. J. Mol. Biol. 75, 281–294.

Ostroff, L.E., Fiala, J.C., Allwardt, B., and Harris, K.M. (2002). Polyribosomes redistribute from dendritic shafts into spines with enlarged synapses during LTP in developing rat hippocampal slices. Neuron 35, 535–545.

Pelechano, V., Chávez, S., and Pérez-Ortín, J.E. (2010). A complete set of nascent transcription rates for yeast genes. PLoS ONE 5, e15442.

Pelechano, V., Wei, W., and Steinmetz, L.M. (2013). Extensive transcriptional heterogeneity revealed by isoform profiling. Nature 497, 127–131.

Pelechano, V., Wei, W., and Steinmetz, L.M. (2015). Widespread co-translational RNA decay reveals ribosome dynamics. Cell 161, 1400–1412.

Potter, M.D., and Nicchitta, C.V. (2002). Endoplasmic reticulum-bound ribosomes reside in stable association with the translocon following termination of protein synthesis. J. Biol. Chem. 277, 23314–23320.

Presnyak, V., Alhusaini, N., Chen, Y.-H., Martin, S., Morris, N., Kline, N., Olson, S., Weinberg, D., Baker, K.E., Graveley, B.R., and Coller, J. (2015). Codon optimality is a major determinant of mRNA stability. Cell 160, 1111–1124.

Reboll, M.R., and Nourbakhsh, M. (2014). Identification of actively translated mRNAs. Methods Mol. Biol. 1182, 173–178.

Sayani, S., Janis, M., Lee, C.Y., Toesca, I., and Chanfreau, G.F. (2008). Widespread impact of nonsense-mediated mRNA decay on the yeast intronome. Mol. Cell 31, 360–370.

Shah, P., Ding, Y., Niemczyk, M., Kudla, G., and Plotkin, J.B. (2013). Rate-limiting steps in yeast protein translation. Cell 153, 1589–1601.

Sheng, M., and Hoogenraad, C.C. (2007). The postsynaptic architecture of excitatory synapses: a more quantitative view. Annu. Rev. Biochem. 76, 823–847.

Sheng, M., and Kim, E. (2011). The postsynaptic organization of synapses. Cold Spring Harb. Perspect. Biol. 3, a005678.

Siwiak, M., and Zielenkiewicz, P. (2010). A comprehensive, quantitative, and genome-wide model of translation. PLoS Comput. Biol. 6, e1000865.

Smith, J.E., Alvarez-Dominguez, J.R., Kline, N., Huynh, N.J., Geisler, S., Hu, W., Coller, J., and Baker, K.E. (2014). Translation of small open reading frames within unannotated RNA transcripts in Saccharomyces cerevisiae. Cell Rep. 7, 1858–1866.

Steward, O., and Schuman, E.M. (2003). Compartmentalized synthesis and degradation of proteins in neurons. Neuron 40, 347–359.

Storz, G., Wolf, Y.I., and Ramamurthi, K.S. (2014). Small proteins can no longer be ignored. Annu. Rev. Biochem. 83, 753–777.

Tuller, T., Carmi, A., Vestsigian, K., Navon, S., Dorfan, Y., Zaborske, J., Pan, T., Dahan, O., Furman, I., and Pilpel, Y. (2010). An evolutionarily conserved mechanism for controlling the efficiency of protein translation. Cell 141, 344–354.

Van Der Kelen, K., Beyaert, R., Inzé, D., and De Veylder, L. (2009). Translational control of eukaryotic gene expression. Crit. Rev. Biochem. Mol. Biol. 44, 143–168.

Warner, J.R., and Knopf, P.M. (2002). The discovery of polyribosomes. Trends Biochem. Sci. 27, 376–380.

Yu, X., and Warner, J.R. (2001). Expression of a micro-protein. J. Biol. Chem. 276, 33821–33825.